Biogeosciences
Discussions

Open Access

EGU

A multi-scale comparison of modeled and observed seasonal methane cycles in northern wetlands

Xiyan Xu[1], William J. Riley[1], Charles D. Koven[1], Dave P. Billesbach[2], Rachel Y.-W. Chang[3,4], Róisín Commane[3], Eugénie S. Euskirchen[5], Sean Hartery[4], Yoshinobu Harazono[6,7], Hiroki Iwata[6,8], Kyle C. McDonald[9,10], Charles E. Miller[10], Walter C. Oechel[11,12], Benjamin Poulter[13], Naama Raz-Yaseef[1], Colm Sweeney[14,15], Margaret Torn[1,16], Steven C. Wofsy[3], Zhen Zhang[15,17], Donatella Zona[11,18]

[1]Earth Sciences Division, Lawrence Berkeley National Laboratory, Berkeley, California, USA;
[2]Biological System Engineering Department, University of Nebraska, Lincoln, Nebraska;
[3]School of Engineering and Applied Sciences, Harvard University, Cambridge, Massachusetts, USA;
[4]Department of Physics and Atmospheric Science, Dalhousie University, Halifax, Nova Scotia, Canada;
[5]Institute of Arctic Biology, University of Alaska Fairbanks, Fairbanks, Alaska, USA;
[6]International Arctic Research Center, University of Alaska Fairbanks, Fairbanks, Alaska, USA;
[7]Graduate School of Life and Environmental Sciences, Osaka Prefecture University, Sakai, Osaka, Japan;
[8]Department of Environmental Sciences, Faculty of Science, Shinshu University, Matsumoto, Nagano, Japan;
[9]Department of Earth and Atmospheric Sciences, CUNY Environmental Crossroads Initiative and NOAA-CREST Institute, The City College of New York, City University of New York, New York;
[10]Jet Propulsion Laboratory, California Institute of Technology, Pasadena, California, USA;
[11]Global Change Research Group, Department of Biology, San Diego State University, San Diego, California, USA;
[12]Department of Environment, Earth and Ecosystems, The Open University, Milton Keynes, U. K. MK7 6AA;
[13]Department of Ecology, Montana State University, Bozeman, MT 59717, USA;
[14]Cooperative Institute for Research in Environmental Sciences, University of Colorado, Boulder, CO, 80304 USA;
[15]NOAA Earth System Research Laboratory, Global Monitoring Division, Boulder, CO, USA;
[16]Energy and Resources Group, University of California-Berkeley, Berkeley, California, USA;
[17]Swiss Federal Research Institute WSL, Birmensdorf 8059, Switzerland;
[18]Department of Animal and Plant Sciences, University of Sheffield, Sheffield S102TN, United Kingdom.

Correspondence to : Xiyan Xu (xxu@lbl.gov)

Biogeosciences
Open Access
EGU
Discussions

47 **Abstract:**
48 Wetlands are the single largest global natural methane (CH_4) source, and emissions
49 between 50°N and 70°N latitude contribute 10-30% to this source. Predictive capability
50 of northern wetland CH_4 emissions is still low due to limited site measurements, strong
51 spatial and temporal variability in emissions, and complex hydrological and
52 biogeochemical dynamics. To explore this issue, we compare wetland CH_4 emission
53 predictions from the Community Land Model 4.5 (CLM4.5-BGC) with site to regional
54 scale observations. A comparison of the CH_4 fluxes with eddy flux data highlighted
55 needed changes to the model's estimate of aerenchyma area, which we implemented and
56 tested. The model modification substantially reduced biases in CH_4 emissions when
57 compared with CarbonTracker CH_4 predictions. CLM4.5 CH_4 emission predictions agree
58 well with growing season (May-September) CarbonTracker Alaskan regional-level CH_4
59 predictions and site-level observations. However, CLM4.5 underestimated CH_4 emissions
60 in the cold season (October-April). The monthly CH_4 mole fraction enhancements due to
61 wetland emissions are also assessed using the WRF-STILT Lagrangian transport model
62 coupled with daily emission priors from CLM4.5 and compared with aircraft CH_4 mole
63 fraction measurements from the Carbon in Arctic Reservoirs Vulnerability Experiment
64 (CARVE) campaign. Both the tower and aircraft analyses confirm the underestimate of
65 cold season CH_4 emissions by CLM4.5. The greatest uncertainties in predicting the
66 seasonal CH_4 cycle are from the wetland extent, cold season CH_4 production and CH_4
67 transport processes. We recommend more cold-season experimental studies in high
68 latitude systems, which could improve understanding and parameterization of ecosystem
69 structure and function during this period. Predicted CH_4 emissions remain uncertain, but
70 we show here that benchmarking against observations across spatial scales can inform
71 model structural and parameter improvements.
72

1 Introduction

Natural wetlands are the single largest natural methane (CH_4) source, contributing up to 34% of global CH_4 emissions (Kirschke et al., 2013). Between 1980 and 2009, estimated global annual CH_4 emissions from wetlands varied from 115 to 231 Tg CH_4 in top-down atmospheric inversion models and 169 to 284 Tg CH_4 in bottom-up process-based land models (Kirschke et al., 2013). Peat-rich bogs and fens lying between 50°N and 70°N constitute about half of the global wetland area, and release 10-30% of the total wetland CH_4 (Wania et al., 2010; Zhuang et al., 2004; Bergamaschi et al., 2009; Riley et al., 2011). Much of the northern wetland area is in the permafrost zone, which stores 1035 ± 150 Pg soil organic carbon for the 0-3m soil depth (Hugelius et al., 2014). When permafrost soils thaw, CH_4 is produced under saturated conditions by anaerobic decomposition of organic carbon by methanogenic bacteria. Once CH_4 is produced, it can be oxidized by methanotrophic bacteria. CH_4 surface emissions occur through several transport pathways: aqueous and gaseous diffusion, ebullition, and aerenchyma diffusion and advection. At any point in the soil, the CH_4 concentration is governed by the balance between CH_4 production in anoxic zones, CH_4 consumption in oxic zones, transport, and atmospheric CH_4 diffusion into the soil.

Many interacting factors (e.g., temperature, thaw depth, soil moisture, depth of the water table, vegetation type) affect CH_4 production and emission. CH_4 production has a positive response to temperature increase (Van Hulzen et al., 1999; van Winden et al., 2012; Hommeltenberg et al., 2014) and laboratory incubations of soil samples from the active layer show that large variability of Q_{10} values for CH_4 production (1.5 to 28, Segers et al., 1998) is related to site-specific peatland type and organic matter quality (Lupascu et al., 2012). CH_4 emissions also show positive temperature dependence above freezing. The temperature dependence of surface CH_4 emission is much stronger than that of respiration and photosynthesis, which indicates increases in both CH_4 emissions and the ratio of CH_4 to CO_2 emissions with seasonal increases in temperature (Yvon-Durocher et al., 2014). The positive temperature dependence of CH_4 emissions may only be valid when CH_4 oxidation is less sensitive to temperature (van Winden et al., 2012). The Q_{10} value for CH_4 oxidation was reported to be 1.4 to 2.1 in northern peat soils (Dunfield et al., 1993). Strong oxidation temperature sensitivity can lead to decreased CH_4 surface emissions with rising temperature (Wang et al., 2014). The positive dependence of CH_4 emissions on soil temperature can be most significant in areas with sufficient soil moisture or a shallow water table (Roulet et al., 1992; Moosavi et al., 1996; Wickland et al., 1999). The dependency of CH_4 emissions on temperature can vanish at high temperature and low water table (Hommeltenberg et al., 2014). At low water table levels, large CH_4 oxidation can mask the CH_4 production temperature sensitivity in the net emissions. CH_4 production under sub-zero temperatures was reported in incubation experiments (Clein and Schimel, 1995; Brouchkov et al., 2003), however, the mechanisms that regulate CH_4 production under cold temperatures have not been clarified.

Soil water content exerts strong control on CH_4 emissions by affecting belowground carbon decomposition and root growth (Iversen et al., 2015). A lowered water table typically reduces CH_4 production and emission, because of a higher aerobic to anaerobic respiration ratio in the soil column and CH_4 oxidation during diffusive

Biogeosciences
Discussions

Open Access

EGU

118   transport through the oxygen-rich surface layer (Whalen and Reeburgh, 1990). If CH_4
119   produced in anoxic zones (e.g., below the water table) is transported to the atmosphere
120   through aerenchyma, the impact of methanotrophy on net CH_4 emissions is diminished
121   (Bartlett et al., 1992; Torn and Chapin, 1993; King et al., 1998; Juutinen et al., 2003;
122   McEwing et al., 2015). The reduced methanotrophic impacts vary with vascular species
123   cover and root density and are more common in tall vegetation, because taller plants have
124   more extensive root systems that enable more methanogenesis and pore water CH_4 to
125   escape to the atmosphere (van Fischer et al., 2010). The methanotrophic impact on
126   ebullition is minimal because bubbling-up of CH_4 from anoxic zones to the surface is
127   very fast (Walter et al., 2006). The correlation between water table depth and CH_4
128   emission can be very weak if the water table drops in an already oxic surface layer
129   (Sturtevant et al., 2012).

130   The seasonal cycle of CH_4 emissions and their physical controls are strongly
131   controlled by the freeze-thaw cycle in northern wetlands, and its regulation of wetland
132   extent. The northern wetland area retrieved from the 19- and 37-GHz passive microwave
133   Special Sensor Microwave/Image (SSM/I) brightness temperature database shows that
134   maximum inundation is usually observed during July, August, and September in north
135   America (48°N-68°N) and between June and September in northern Eurasia (Mialon et
136   al., 2005). The inundation dynamics retrieved from SSM/I and ISCCP observations, ERS
137   scatterometer responses, and AVHRR visible and near-infrared reflectance also show that
138   maximum inundation occurs in July and August in northern boreal regions (55°N-70°N)
139   (Prigent et al., 2007). The inferred wetland extent increases rapidly during the spring
140   thaw period and shrinks again during the fall freeze period; though it is unclear at large
141   scales how much of this seasonal cycle is due to changes in the areal fraction of land in
142   which water ponds at the surface versus changes in the phase of that water. The
143   interannual variability of high-latitude summer wetland extent is very small. Larger
144   interannual variability during the intermediate seasons arises from the large variability of
145   the timing and extent of snowmelt and accumulation (Mialon et al., 2005). For boreal
146   bogs north to 50°N, the variation in wetland area contributed about 30% to the annual
147   emissions and can explain the interannual variation in regional CH_4 emissions (Ringeval
148   et al., 2010).

149   Site measurements have shown great variability in seasonal CH_4 emissions
150   (Wilson et al., 1989; Mastepanov et al., 2008; 2013; Zona et al., 2016). In the late fall to
151   winter, the surface water or shallow peat zone are frozen, and CH_4 produced below the
152   frozen layer can be trapped. Only a small portion of the trapped CH_4 is oxidized because
153   of low oxygen concentrations below the frozen layer (Mastepanov et al., 2008). Observed
154   CH_4 emissions during spring thaw are highly variable and contribute substantially to total
155   annual emissions. CH_4 fluxes during the spring thaw period contributed 11% to the
156   annual budget over an aapa mire in Finnish Lapland (Hargreaves et al., 2001). The
157   emission amounts can be 24% of the total annual emissions during the spring period after
158   snowmelt next to an open pool in Caribou Bog, Maine, while the proportion can be as
159   high as 77% in the adjacent upland area (Comas et al., 2008). In the non-inundated
160   upland tundra, the cold season (September to May) emissions account for more than 50%
161   of the annual CH_4 emissions (Zona et al., 2016). Although wetlands can contribute a
162   large proportion of annual CH_4 emissions during the cold season, the seasonal peak of
163   CH_4 emissions is usually observed in the summer (Pickett-Heaps et al., 2011; Zona et al.,

164 2016). A transport model combined with flight measurements showed the peak CH_4
165 emission to be in July-August in the Hudson Bay Lowlands (Pickett-Heaps et al., 2011).
166 Although the recorded emission pulses during spring thaw and late fall (Song et al., 2012;
167 Tokida et al., 2007; Rinne et al., 2007; Mastepanov et al., 2008; 2013) may be more
168 localized and of minor importance to annual emissions (Chang et al., 2014; Rinne et al.,
169 2007), the pulses indicates the complexity and heterogeneity in the seasonal CH_4 cycle.

170 Many modeling studies have shown that there is large uncertainty in predictions
171 of spatial patterns of CH_4 emissions from natural wetlands at the regional and global
172 scales (Melton et al., 2013; Bohn et al., 2015). This uncertainty can be roughly split into
173 poor knowledge of water table and soil moisture dynamics versus poor knowledge of
174 CH_4 fluxes per unit area of land with a given water table depth or soil moisture state; both
175 contribute substantially to the overall uncertainty. One approach to reducing this overall
176 uncertainty is to focus on the seasonal cycles of CH_4 emissions at the site scale (where
177 inundation dynamics can be more easily constrained) versus at larger scales to ask
178 whether model predictions and errors are consistent across these scales. The temporal
179 dynamics of CH_4 emissions over the season cannot be ignored when calculating long-
180 term CH_4 budgets (Morin et al., 2014). To investigate the seasonal cycle of CH_4
181 emissions in northern wetlands and the underlying processes in a climate model context,
182 we evaluated and modified the CH_4 biogeochemistry module in the Community Land
183 Model (CLM 4.5). Seasonal cycles of CH_4 emissions in Alaskan wetlands are analyzed
184 based on the modified model predictions, CH_4 emission measurements at high-latitude
185 sites, CarbonTracker CH_4 emission estimates, and atmospheric inversion estimates of
186 surface CH_4 emissions from data collected in the Carbon in Arctic Reservoirs
187 Vulnerability Experiment (CARVE).

188 **2 Data and Methods**

189 **2.1 Models description**

190 **2.1.1 CH_4 model in CLM4.5-BGC**

191 The CH_4 biogeochemistry model used here (CLM4Me; Riley et al. (2011)) has
192 been coupled to the revised land model CLM4.5, which includes numerous changes to
193 vegetation, soil biogeochemistry, and hydrology from the CLM4.0 in which CLM4Me
194 was originally developed. CLM4Me includes representation of CH_4 production,
195 oxidation, and transport through the soil column. Transport includes multiple pathways:
196 aerenchyma transport, ebullition, and aqueous and gaseous diffusion. Aerenchyma is the
197 most efficient pathway for gas exchange between the soil and atmosphere in wetlands or
198 aquatic environments, through which atmosphere O_2 is supplied to roots and the
199 rhizosphere while CH_4 is removed from the soil to shoots and the atmosphere. In
200 CLM4Me, aerenchyma transport is parameterized as gaseous diffusion in response to a
201 concentration gradient between the soil layer (z) and the atmosphere (a) as:

202

203 $A = \dfrac{C(z) - C_a}{\dfrac{r_L z}{D_p T \rho_r} + r_a}$,   (1)

204 where D (m^2 s^{-1}) is the free gas diffusion coefficient, $C(z)$ (mol m^{-3}) is the gaseous
205 concentration at depth z, r_L is the ratio of root length to depth, p (-) is porosity; T (m^2 m^{-2})
206 is specific aerenchyma area, r_a (s m^{-1}) is the aerodynamic resistance between the surface
207 and the atmospheric reference height, and r_r (-) is the root fraction in the soil layer. The
208 aerenchyma area T is seasonally varying with phenology S (described below):

209

210 $$T = \frac{f_N N_a S}{0.22} \pi R^2 ,$$ (2)

211

212 where N_a (mol m^{-2} s^{-1}) is annual net primary production(NPP), R (2.9x10^{-3} m) is the
213 aerenchyma radius, f_N is the belowground fraction of current NPP, and the factor 0.22 is
214 the amount of C per tiller. The dimensionless term S is included in CLM4Me to capture
215 seasonal cycles of aerenchymous tissues. In the absence of data on phenology of
216 aerenchyma, S was originally taken as the leaf area index (LAI). As discussed below,
217 however, this assumption leads to seasonal cycle CH$_4$ emission biases.

218   The CH$_4$ transport through aerenchyma is most sensitive to aerenchyma area in
219 saturated conditions, and decreases with increasing aerenchyma area, because increased
220 O$_2$ fluxes through aerenchyma cause more CH$_4$ oxidation in the rhizosphere (Riley et al.,
221 2011). Meng et al. (2012) tested plant functional type (pft)-specific fine root carbon (C_{FR})
222 as a proxy of aerenchyma area and found that aerenchyma area dependence on C_{FR} leads
223 to about 39% increases in global annual CH$_4$ emissions. In Meng et al., (2012)'s study, an
224 early spring spike in CH$_4$ emission through aerenchyma transport was shown at a
225 Michigan site in both LAI and C_{FR} based aerenchyma area. Our analysis shows that the
226 simulated CH$_4$ burst through aerenchyma transport during spring thaw is very common in
227 areas experiencing winter dormancy. In CLM4Me, CH$_4$ production is proportional to grid
228 cell-averaged heterotrophic respiration (HR) from soil and litter, adjusted by soil
229 temperature, pH, redox potential, and variation of seasonal inundation fraction. In the
230 model, CH$_4$ production starts when the soil temperature is above the freezing point.
231 However, CLM4.5 LAI lags behind the primary thaw day, which results in a very low
232 aerenchyma area and thus low aerenchyma transport of O$_2$ into the soil during spring
233 thaw period. Only a very small portion of the CH$_4$ produced in the soil column is
234 oxidized, allowing a large fraction of CH$_4$ to be transported to the surface by aerenchyma.
235 The low oxidation rate also occurs when aerenchyma area is calculated with C_{FR}.

236   The uncertainty in representing the seasonality of aerenchyma area is due to (1)
237 poor current understanding of root dynamics and their control on aerenchyma area and (2)
238 scant relevant observations. In tundra, the aboveground production is often not a good
239 proxy for belowground production, because the soil temperature peaks later in the
240 growing season than solar irradiance (Sullivan and Welker, 2005; Sloan, 2011). Further,
241 root dynamics are strongly dependent on species. Root growth of *Eriophorum*
242 *angustifolium* may not be delayed when soil temperature is near 0°C (Chapin, 1974;
243 Billing et al., 1977), while *Dupontia Fischeri* produces many fewer root tips at these low
244 temperatures. In *Eriophorum vaginatum*, fine root growth is lagged significantly behind
245 the aboveground spring growth flush (Kummerow and Russell, 1980).

246   To eliminate the possible bias in the seasonal variation of roots and the extremely

247   low oxidation rate which caused CLM4Me to predict a large inundated area CH_4 burst
248   from inundated areas during the spring thaw, we modified the model parameter S to be
249   constant, which is used in the aerenchyma area estimation. We constrained S using global
250   total CH_4 emissions estimated by top-down and bottom-up simulations during 2000-2009
251   (Kirschke et al., 2013) and site-level measurements. We exclude the CH_4 emission from
252   non-inundated area for the analysis of seasonal dynamics because the model shows very
253   small seasonal contribution of CH_4 emission from non-inundated areas globally (Fig. 1).
254   This CH_4 emission pulse from the non-inundated area, which may be related to soil
255   moisture anomalies during spring thaw, has not been experimentally validated, but can
256   lead to large biases in simulated CH_4 emissions from northern high latitudes (>50°N) in
257   May and June (Fig. 1a and 1b). This simplification of the model produced seasonal cycles
258   that did not contain the large springtime CH_4 emission bursts, and we therefore used this
259   modified version for all experiments here.

260   The default method for calculating inundation fraction (F_{def}) remains the same as
261   described in Riley et al. (2011), which applied a simple inversion model to represent the
262   spatial inundation:

263

264    $$F_{def} = p_1 e^{-z_w/p_2} + p_3 Q_r \,,\qquad\qquad\qquad (3)$$

265

266   The three parameters (p_1, p_2, p_3) are optimized with the inundation map by Prigent et al.
267   (2007). z_w is simulated water table depth (m) and Q_r is surface runoff (mm s^{-1}). We also
268   applied an estimate of inundation fraction F_{S+G} (Poulter et al., In Review) derived from
269   seasonal cycle of inundation fraction from the Surface WAter Microwave Product Series
270   Version 2.0 (SWAMPS, Schroeder et al., 2015) developed at the NASA Jet Propulsion
271   Laboratory with the Global Lakes and Wetlands Dataset (GLWD, Lehner and Doll, 2004)
272   to discuss the potential uncertainties in CH_4 emissions caused by wetland area.

273   Our model is driven by half-degree CRUNCEP V5 6-Hourly Atmospheric
274   Forcing dataset (1901-2013) (http://dods.extra.cea.fr/data/p529viov/cruncep/readme.htm).
275   Monthly wetland CH_4 emissions are simulated between the year 2000 and 2012 during
276   which F_{S+G} is available. The monthly CH_4 emissions in half-degree resolution are
277   regrided to 1°×1° and averaged longitudinally to compare with CarbonTracker predicted
278   CH_4 fluxes. Daily wetland CH_4 emissions are simulated for year 2012 and 2013 to
279   calculate the atmospheric enhancements of CH_4 due to modeled surface emissions.

280   **2.1.2 WRF-STILT modeling of CH_4 transport**

281   We simulate the atmospheric CH_4 mole fraction enhancements due to wetland
282 emissions by combining the CLM4.5 predicted daily surface emissions with the land
283 surface influences ("footprint") calculated by the Weather Research and Forecasting-
284 Stochastic Time-Inverted Lagrangian Transport (WRF-STILT) model (Henderson et al.;
285 2015). WRF-STILT estimates the upwind surface influence along the flight track of the
286 CARVE aircraft by releasing 500 particles at the point of flight measurement and
287 allowing them to stochastically disperse in reverse time over 10 days (Henderson et al.,
288 2015). The resolution of the resulting footprint sensitivity used in this study
289 is 0.5 °×0.5°, covering 30-90°N, circumpolar. However, we assume that CH_4
290 transported from areas outside of Alaska are most likely mixed thoroughly in the
291 atmosphere before they reach Alaska, and therefore only contribute to the background
292 abundance of CH_4.

293 **2.2 Measurements of CH_4**

294 **2.2.1 Site-Scale Observations**

295   We compare CLM4.5 CH_4 emission predictions with data obtained from
296 published studies and recent measurements of northern hemisphere static chamber (SC)
297 measurements at 10 sites and eddy covariance (EC) measurements at 10 sites, of which 8
298 are in Alaska (Supplement Table S1). The eddy covariance measurements in Alaska (Fig.
299 S2) are obtained at the Barrow Environmental Observatory (BEO1) tower operated by the
300 Next Generation Ecosystem Experiment (NGEE)-Arctic group; Barrow Environmental
301 Observatory tower (BEO2), Biocomplexity Experiment South (BES) tower, Climate
302 Monitoring and Diagnostics Laboratory (CMDL) tower, Atqasuk (ATQ) tower and
303 Ivotuk (IVO) tower operated by Global Change Research Group at San Diego State
304 University (Zona et al., 2016); tower in Fairbanks (FAI, Iwata et al., 2015) operated by
305 International Arctic Research Center, the University of Alaska Fairbanks; and tower at
306 the Imnavait Creek watershed (IMN, Euskirchen et al., 2012). Monthly means are
307 calculated across each observational record to compare to predicted mean seasonal CH_4
308 cycle. We discarded the monthly mean if the number of valid measurement days is less
309 than half a month.

310 **2.2.2 Comparisons to Airborne Measurements**

311   The regionally integrated CH_4 mole fraction enhancements over Alaska were
312 calculated from the CH_4 mole fractions measured by NOAA and Harvard Picarro
313 spectrometers aboard a NASA C-23B aircraft (N430NA) during CARVE aircraft flights
314 (Chang et al., 2014). The Harvard CH_4 measurements were gap filled with the NOAA
315 CH_4 measurements to create a continuous 5-s time series. The flight measurements were
316 conducted on selected days from May to September in 2012 and April to October in 2013
317 during the Carbon in Arctic Reservoirs Vulnerability Experiment (CARVE) campaign,
318 for a total of 31 flight days in 2012 and 43 flight days in 2013 (Fig. S1 and Table S2).
319 The measurements of CH_4 with concurrent CO mole fractions above 150 ppb are
320 excluded to remove possible CH_4 production from biomass burning. In Alaska,
321 atmospheric boundary layer depth is in the range of 1100-1600 m above ground level
322 (agl) during April and October according to COSMIC satellite and Radiosonde data

323   (Chan and Wood, 2013). We assume that the observed concentration fluctuations below
324   500m agl can be used to infer the variation of surface CH_4 fluxes; the measurements
325   above 1600 m agl are used to infer background mole fraction of CH_4. The monthly mean
326   enhancements in observed atmospheric CH_4 mole fraction is compared to that estimated
327   from the CLM4.5 CH_4 enhancements.

328   **2.2.3 Comparisons to Global-Scale Inversions**

329   To compare our methane emissions with global and regional scale inversions, we
330   use monthly regional CH_4 emissions predicted by CarbonTracker (Peters et al., 2007;
331   Bruhwiler et al., 2014) at 1°×1° resolution. In CarbonTracker estimates, the natural CH_4
332   emissions correspond to wetlands, soils, oceans, insects, and wild animals. To examine
333   the land CH_4 emissions only, we apply the CLM land mask to exclude the inferred
334   CarbonTracker CH_4 emission from the ocean surface. CarbonTracker CH_4 estimates are
335   available from January 2000 through December 2010; we therefore limit comparisons
336   against the CLM4.5 predictions to this period.

337   **3 Results and Discussion**

338   **3.1 Model constraints and comparison with observations**
339   We assessed the sensitivity of the modeled CH_4 fluxes to parametric uncertainty
340   in the constant dimensionless factor S, as described in the Methods. S has a direct effect
341   on the magnitude of modeled CH_4 emissions via its control of oxygen diffusion through
342   the soil column and thus CH_4 oxidation. When $S = LAI$, the very low LAI in the spring
343   thaw period leads to low oxidation and consequently overestimated CH_4 net emissions.
344   During the growing season, the model overestimates LAI at high latitude (Tian et al.,
345   2004) leading to high oxidation and consequently underestimated net CH_4 emissions (Fig.
346   1e and f). However, few observations of aerenchymous tissue biomass are available to
347   provide an *a priori* constraint to this value. Our goal here is to use a reasonable value of
348   this parameter, not to fully characterize the uncertainty of the parameter choice on CH_4
349   emissions.

350   Based on a comparison of the globally integrated CH_4 flux with other global
351   estimates, we choose $S=4$, which resulted in an estimated annual total CH_4 emission of
352   228 [Inter-annual Variability (IAV): 221- 239] Tg CH_4 yr^{-1} with F_{def} and 206 [IAV: 200-
353   217] Tg CH_4 yr^{-1} with F_{S+G} during the period 2000 - 2009. The top-down and bottom-up
354   models have estimates of CH_4 emissions from natural wetlands of 175 [IAV: 142-208]
355   Tg CH_4 yr^{-1} and 217 [IAV: 177-284] Tg CH_4 yr^{-1}, respectively, during the same period
356   (Kirschke et al., 2013). The mean CH_4 emission predicted by CLM4.5 is about 42 Tg
357   CH_4 yr^{-1} lower than the original CLM4Me prediction (annual mean of 270 Tg CH_4 yr^{-1}
358   from 1948 to 1972), but slightly larger than the mean value from other bottom-up and
359   top-down models. The disagreement between studies with different models is as large as
360   66% (Kirschke et al., 2013), hence our estimate is well within the range of values from
361   top-down constraints and underscores the uncertainty involved in using such a constraint
362   in inferring model parameters.

Biogeosciences
Discussions

Open Access

EGU

363   Compared with CarbonTracker predictions, CLM's biases of underestimated
364   growing-season CH_4 emissions north of 56°N and biases of overestimated CH_4 emissions
365   in 2-53°N and 34-56°S are reduced when using $S = 4$ compared to the default
366   parameterization (Fig. 1d and f). For the global zonal mean, the CLM CH_4 prediction
367   biases are reduced with F_{S+G} (RMSE=25 ng C m^{-2} s^{-1}) compared with F_{def} (RMSE = 31 ng
368   C m^{-2} s^{-1}). With F_{S+G}, the biases are much reduced in 2-50°N and 30-58°S. However,
369   negative CH_4 emission biases in the tropics remain (Fig. 1c and 1e). The differences in
370   CH_4 emissions using SWAMPS-GLWD and CLM4.5 predicted inundation fraction
371   implies that the prediction uncertainties are not only from the biogeochemical
372   parameterization but also from the wetland extent, consistent with several recent model
373   inter-comparison analyses (Melton et al., 2013; Bohn et al., 2015). In Alaska, the
374   predicted annual CH_4 emissions between 2000 and 2010 are 1.47±0.20, 1.58±0.07, and
375   1.12±0.05 Tg CH_4 yr^{-1} for CarbonTracker, CLM4.5 with F_{S+G}, and CLM4.5 with F_{def},
376   respectively. Although our predicted annual emissions are reasonable compared with
377   most land surface model predictions, the May to September predictions are about 50-70%
378   of the emissions estimated using an atmospheric inversion based on CARVE
379   observations of 2.1± 0.5 Tg CH_4 yr^{-1} (Chang et al., 2014).

380   **3.2 Seasonal CH_4 Cycle**

381   **3.2.1 Site level comparison**

382   The mean seasonal cycle of predicted CH_4 emissions is calculated from the 2000-
383   2012 monthly mean in a 0.5°×0.5° grid cell where site measurements exist, while the
384   seasonal cycle of site measurements is calculated for the measurement years. If multiple
385   measurement sites and multiple measurement years with the same measurement method
386   (SC or EC) exist within a given grid cell, the observations are averaged to create a grid
387   cell mean value that can be directly compared with the modeled value for that grid cell.
388   In the 10 site-level static chamber measurements at saturated sites (Fig. 2a-l), the
389   seasonality is well predicted by the revised CLM4.5 CH_4 model at most sites.
390   Measurements and predictions show the peak emission month to be July or August at
391   most sites, except the site in Michigan, USA (Fig. 2f) where the model successfully
392   predicted the peak emissions in May. However, the model misrepresents the seasonality
393   at the Stordalen (Sweden) (Fig. 2a and k) and the Boreas NSA (Canada) (Fig. 2i) site. At
394   the Ruoergai (China) (Fig. 2j), the model does not show a strong seasonal variation from
395   April to September, and notably underestimates the growing season CH_4 emissions. The
396   underestimation of growing season emissions is also found in the Minnesota (USA),
397   Michigan (USA), and Boreas NSA (Canada) sites (Fig. 2d, 2e, 2f and 2h). The sites
398   experiencing soil frost with valid measurements in the cold season demonstrate the
399   underestimation of CLM4.5 CH_4 emission predictions during this period (Fig. 2a, 2d, 2e
400   and 2i).

401   The eddy covariance measurements from four sites, the BEO1, BEO2, BES, and
402   CMDL sites are in the same model grid cell, therefore, the measurements in these four
403   sites are aggregated to the same grid cell as that of Alaska (Fig. 2m). As the footprints of
404   the measurement towers were not estimated, all the modeled CH_4 emissions at eddy
405   covariance sites are weighted with an observationally estimated seasonal-invariant range

406 of inundation faction: Stordalen: 80-100%; Boreas SSA: 50-90%; Barrow: 60-100%;
407 Atqasuk: 10-30%; Ivotuk: 5-25%; Fairbanks: 0.5-2.5% and IMN: 5-25%. Measurements
408 at the Stordalen site (Fig. 2a and k) show very different CH_4 emission patterns in
409 seasonality and magnitude for different years and measurement methods. The model
410 significantly underestimates CH_4 emissions even with the maximum fraction of
411 inundation in Stordalen (Fig. 2k). In comparison with the static chamber measurements at
412 Alaska (Fig. 2h), the model predicts a much shorter CH_4 emission season at the non-
413 inundated sites (Fig. 2m-q). The estimated CH_4 emissions begin in April at Ivotuk,
414 Fairbank, and Imnavait. At the northern sites, Barrow and Atqasuk, the estimated CH_4
415 emissions begin in May. In the short emission season, the model underestimates CH_4
416 emissions in June and July at Barrow and Atqasuk and in July at Imnavait, even with the
417 maximum inundation estimation. While the cold-season measurements at Barrow,
418 Atqasuk, and Ivotuk show large CH_4 emissions from October to April in agreement with
419 the static chamber measurements at the sites with cold season soil frost, predicted CH_4
420 emissions end in October at all the Alaskan sites. The largest monthly mean emissions in
421 Alaska cold season are 24.8 ± 9.0 mg CH_4 m^{-2} day^{-1} measured in October at Ivotuk.

422 A number of factors affect the correspondence between site-level CH_4 emission
423 observations and CLM predictions (Fig. 2), including: (1) we used reanalysis climate
424 forcing data which may lead to some of the differences with the site observations; (2) we
425 used the model's default surface characterization, which is unlikely to exactly match the
426 actual vegetation and soil properties; (3) the spatial and temporal coverage of the site data
427 are sparse; (4) the inter-annual variation of wetland CH_4 emission can be significant; (5)
428 the method of measuring CH_4 fluxes varied from site to site and (6) the seasonal fraction
429 of inundation in eddy covariance tower footprint is unknown. We also expect differences
430 between our CLM4.5 predictions and those reported in Riley et al., (2011) at the site-
431 level comparison, because: (1) simulations in this study were done at higher resolution
432 ($0.5° x 0.5°$) than those in Riley et al. (2011) ($1.9° x 2.5°$); (2) the current simulations are
433 forced by CRUNCEP climate, while Riley et al., (2011) simulations were forced with
434 Qian et al., (2006) climate; (3) the S parameter is changed, as discussed above; and (4)
435 the overall water and carbon cycles of CLM changed substantially between CLM4.0 and
436 CLM4.5 (Koven et al., 2013). The site-level discrepancies occur because of the
437 uncertainties discussed above and those arising from other parameters (Riley et al., 2011),
438 including: Q_{10} of CH_4 production and oxidation, CH_4 half-saturation oxidation coefficient,
439 O_2 half-saturation oxidation coefficient, maximum oxidation rate of CH_4 oxidation, and
440 impact of pH and redox potential on CH_4 production.

441 **3.2.2 Regional CH_4 emissions comparison**

442 The biases between CLM4.5 and CarbonTracker CH_4 emissions vary with latitude
443 (Fig. 3). The aggregated F_{S+G} led to larger CH_4 emission biases in Alaska (RMSE = 4 mg
444 CH_4 m^{-2} day^{-1}) compared to the CH_4 prediction with F_{def} (RMSE = 3 mg CH_4 m^{-2} day^{-1}),
445 although it led to smaller global CH_4 emission biases. In Alaska between 58-66°N during
446 the growing season, CLM4.5 using F_{def} has good agreement with CarbonTacker
447 predictions. In this region, CH_4 emissions begin in May, peak in July and August,
448 end in October (Fig. 4). In May and June, CarbonTacker shows a weak CH_4 sink ($\sim o[10^{-1}-1]$ ng C m^{-2} s^{-1}) in contrast to a CLM4.5 predicted weak CH_4 source ($\sim o[1]$ ng C m^{-2} s^{-1})

450   with F_{def} and stronger CH_4 source (~$o[10^1]$ ng C m^{-2} s^{-1}) with F_{S+G} in the interior region
451   of Alaska (Interior Alaska) between 63°N-66°N . We hypothesize that this discrepancy
452   occurs because of the difference in the two wetland datasets and the accounting of CH_4
453   emissions from the non-inundated areas in CarbonTracker. Net CH_4 consumption occurs
454   at dry sites where oxygen is available in the top soil layers (Wickland et al., 1999);
455   however, CH_4 fluxes from the non-inundated areas which could be substantial (Zona et
456   al., 2016) are excluded in CLM4.5 predictions shown in Fig. 3, as described in Methods.
457   Interior Alaska has a highly continental climate with warm and relatively dry summers
458   and extremely cold winters. The weak CH_4 source in the dry summer is thus caused by a
459   reduced wetland extent in Interior Alaska. Interior Alaska experiences the most rain
460   events in autumn, mainly in August and September (Hinzman et al., 2006), which
461   restores some of the extent of wetlands and leads to increases in CH_4 emissions in August
462   and early September. CarbonTracker successfully represented the restored wetland in
463   August and September but not CLM4.5 (Fig. 3 and 4). The autumn emission period is
464   very short and ends with the onset of winter, resulting in a strong drop in CH_4 emissions
465   in October.

466   The CLM4.5 underestimation of northern (> 68°N) Alaska site-level CH_4
467   emissions during the growing season at some sites is confirmed with comparison to
468   CarbonTracker inversions (Fig. 3b). In southern and northern coastal Alaska, CLM4.5
469   predicts a much shorter CH_4 emission season and a smaller magnitude of CH_4 emissions
470   than CarbonTracker. The main season of strong underestimation by CLM4.5 is from May
471   to July with the maximum underestimation of about 9.2 mg CH_4 m^{-2} day^{-1} in June. The
472   underestimated CH_4 emissions occur with both F_{S+G} and F_{def} in the north of 68°N.
473   During the cold season from October to April, CLM4.5 predictions with F_{S+G} or F_{def} are
474   consistently smaller than CarbonTracker estimates across all the latitudes. The mean
475   underestimation of cold season CH_4 emission is less than 1 mg CH_4 m^{-2} day^{-1}, which is
476   much smaller than the underestimation we found compared to site level measurements.
477   In comparison with CarbonTracker, CLM4.5 predicted 0.46±0.07Tg and 0.39±0.08Tg
478   less Alaska wide CH_4 emissions in cold season (October to April) with F_{S+G} and F_{def},
479   respectively.

480   The CarbonTracker inversions suggest 21.9±3.2% of the annual Alaska CH_4
481   emissions occur during the cold season, while CLM4.5 predicts only 3.5±1.3% and
482   8.3±3.0% (with F_{def} and F_{S+G}, respectively) occur during the cold season. When
483   September and April are included in the "cold season", the contribution is increased to
484   45.3±4.5% by CarbonTracker, which is slightly smaller than the cold season contribution
485   (50±9%) inferred from site-level (BEO2, BES, CMDL, ATQ and IVO) measurements
486   (Zona et al., 2016). The September-April contributions to annual emissions predicted by
487   CLM4.5 are 32.1±8.1% and 40.1±14.7% of the predicted annual emissions with F_{S+G} and
488   F_{def}, respectively. Although CH_4 fluxes from the ocean surface are excluded, we cannot
489   exclude some influence of coastal grid cells on the CarbonTracker estimates.

490   The atmospheric CH_4 mole fraction enhancements calculated from CLM4.5
491   predicted CH_4 emissions are lower than the CARVE measured CH_4 mole fraction
492   enhancements (Fig. 5). However, in contrast to the emission underestimations that only
493   occur from May to July, the monthly atmospheric CH_4 mole fraction enhancements are
494   underestimated throughout the year, with a maximum underestimation in August (Fig.

5a). The CARVE measured peak mole fraction enhancement due to surface CH_4
emissions is in August for both 2012 and 2013. Although CLM4.5 predicted the peak
CH_4 mole fraction enhancement in August, 2012, predicted seasonal CH_4 mole fraction
enhancements are much smaller in 2013 and peaks in September. The underestimation of
cold season mole fraction CH_4 enhancements by CLM4.5 leads to 24.0±9.2 ppb and
18.9±17.3 ppb lower CH_4 mole fraction enhancements in April and October 2013,
respectively. From April to October, the two-year mean monthly atmospheric CH_4 mole
fraction enhancements are underestimated by 15 ppb in WRF-STILT-CLM model
predictions. The underestimation may not be attributed to anthropogenic CH_4 source
because ▭ excluded both observed and modeled CH_4 mole fraction enhancements when
[CO]>150 ppb, given that anthropogenic CH_4 mole fraction enhancements are
consistently correlated to CO mole fraction enhancements (Zona et al., 2016). The large
standard deviation of CARVE observed CH_4 mole fraction enhancements implies that the
CH_4 emissions have large spatial and temporal variability. The CLM4.5 predictions are
generally within the observed range of variation except in April and May in 2013.

The very low cold season CH_4 emission predictions at site and regional scales
occurs because of the assumed temperature sensitivity for CH_4 production when the soil
temperature of a given layer is at or below freezing (i.e., no CH_4 production occurs in that
soil layer). The multi-layer structure of CLM4.5 can in principle generate CH_4 emissions
deeper in the soil after the surface has frozen, though even then, modeled diffusion rates
through frozen surface layers are low. Although the measurements show winter CH_4
emissions, it remains uncertain whether these emissions are from production at low
temperature or residual CH_4 from the end of the growing season. Understanding which of
these is occuring is important for diagnosing how to improve model representation of the
processes responsible for the wintertime fluxes. The cold season underestimation by
CLM4.5 is also partly attributed to the low wetland area during this period at high
latitudes (currently, F_{def} is set to zero when snow is present). Given the current
observations of CH_4 emissions during the cold season, we believe these two factors need
to be re-evaluated in CLM4.5.

3.3 Interannual variation of CH_4 cycle

The CLM4.5 simulated Alaska CH_4 emissions using F_{def} are in very good
agreement with CarbonTracker-CH_4 emission in the growing season but biased in the
cold season (Fig. 6). The largest growing season discrepancies occur in 2006 and 2007.
Bruhwiler et al. (2014) attributed the CarbonTracker 2007 CH_4 emission anomaly to
warmer temperatures and higher than normal precipitation. However, the CRUNCEP
reanalysis data we used to force CLM4.5 do not have a positive precipitation anomaly in
either 2006 or 2007 (Fig. 7a). In contrast, there is a strong negative precipitation
anomaly in 2007. The obvious wet years (2000, 2005, 2008, 2011 and 2012) in the
CRUNCEP reanalysis data are not directly related to the predicted and measured wetland
area anomaly or CH_4 emission anomaly. The mean air temperature in 2007 is only
slightly higher than 2000-2012 mean air temperature (Fig. 7b). The correlation analysis
implies that the model predicted interannual CH_4 variation is mainly explained by
temperature variation (Fig. 8a, r=0.86, P=0.0007), followed by the default wetland extent
(F_{def}) variation (Fig. 8b, r=0.65, P=0.03), but weakly explained by SWAMPS-GLWD
wetland extent (F_{S+G}) variation (r=0.44, P=0.17) and precipitation variation (r=0.18,

540   P=0.58). When the CH_4 predictions are calculated with F_{S+G}, correlation between the
541   interannual variation of CH_4 and variation in F_{S+G} (r=0.18, P=0.59), precipitation (r=0.36,
542   P=0.29), and temperature (r=0.32, P=0.33) are substantially reduced. Interannual
543   variation of CH_4 emissions by CarbonTracker are not well correlated to SWAMPS-
544   GLWD wetland extent variation (r=0.33, P=0.32), variations in CRUNCEP temperature
545   (r=-0.23, P=0.49), or precipitation (r=-0.06, P=0.86).

4 Concluding remarks

547   We implemented and tested needed changes to the estimate of aerenchyma area in
548   CLM4.5. The modeled and measured CH_4 emissions and enhancements in atmospheric
549   mole fractions of CH_4 are used to analyze the seasonal wetland CH_4 emission cycle in
550   Alaska. Both the measurements and model predictions show large latitudinal variability
551   of CH_4 seasonal cycles. At the site level, CLM4.5 generally captures the seasonality in
552   growing season CH_4 emissions. However, comparing eddy covariance CH_4 observations
553   with the model predictions is complicated by the unknown fraction of inundation in the
554   footprint of the measurement tower, which may cause large variations in CH_4 emission
555   predictions. Measurements from the sites experiencing wintertime soil frost imply that
556   CH_4 emissions continue in the cold season (October to April). The likely incorrect
557   treatment of CH_4 production under soil frost in CLM4.5 leads to underestimates of the
558   wintertime emissions. This conclusion is confirmed by the discrepancies between
559   CLM4.5 and CarbonTracker predictions, although the cold season discrepancies between
560   CLM4.5 and CarbonTracker are much smaller than the discrepancies between CLM4.5
561   and site-level measurements. The differences between the seasonality predicted by
562   CLM4.5 and CarbonTracker vary with time and latitude, although the Alaska area-
563   integrated CH_4 emissions agree well. Besides the strength of wintertime CH_4 emissions,
564   the main discrepancies between CLM4.5 and CarbonTracker estimates are northern and
565   southern coastal area CH_4 emissions. The inundation area leads to uncertainties in
566   predictions of seasonal and interannual variability of CH_4 emissions, as has been
567   concluded elsewhere. Compared with the CLM4.5 predicted inundation area, the
568   aggregated F_{S+G} inundation led to smaller global CH_4 emission biases than F_{def} (RMSE
569   dropped from 31 ng C m^{-2} s^{-1} to 25 ng C m^{-2} s^{-1}) between CLM4.5 and CarbonTracker. In
570   contrast, the F_{S+G} inundation area increased seasonal emission biases in Alaska by
571   increasing RMSE from 3 to 4 mg CH_4 m^{-2} day^{-1} compared with the CLM4.5 predicted
572   inundation. The larger SWAMPS-GLWD inundation area leads to much stronger Alaska
573   wide annual CH_4 emissions compared to those calculated from the default predicted
574   inundation area. CLM4.5 predictions show that the interannual variations of CH_4
575   emissions are correlated with the reanalysis air temperature and wetland extent variation.
576   In contrast, interannual variation in CarbonTracker CH_4 emissions is weakly related to
577   interannual variation in SWAMPS-GLWD wetland area and reanalysis precipitation and
578   temperature.

579   The CLM4.5 CH_4 module constrained from global total annual CH_4 emissions
580   does not accurately represent the seasonal cycles at the regional and site scale seasonal
581   cycles due to large temporal and spatial heterogeneity in surface CH_4 emissions and
582   wetland extent. Further improving the CH_4 biogeochemical model at the seasonal and
583   annual time scales requires further extensive experiments to better understand climate
584   controls on above- and below-ground physiological processes and how vegetation

Biogeosciences
Discussions

Open Access

EGU

585   controls gaseous transport (e.g. CH_4 production under low temperatures). Although cold
586   season site-level measurements are rare, the large discrepancies in winter emissions
587   between CLM4.5 and CarbonTracker predictions and site measurements indicate that
588   studies on winter ecosystem activities and wetland evolution in high latitude would be
589   valuable.

590

591

References

Alavala, P. C. and Kirchoff, V. W. J. H.: Methane fluxes from the Pantanal floodplain in Brazil: Seasonal variation, in: Non-CO_2 Greenhouse Gases: Scientific understanding, control and implementation, edited by: Goossens, A., De Visscher, A., Boeckx, P., and Van Cleemput, O., Kluwer Academic Publishers, Netherlands, 95–99, 2000.

Bartlett, K. B., Crill, P. M., Sass, R. L., Harriss, R. C., Dise, N. B.: Methane emissions from tundra environments in the Yukon-Kuskokwim delta, Alaska, J. Geophys. Res., 97D, 16645–16660, 1992.

Bergamaschi, P., Frankenberg, C., Meirink, J. F., Krol, M., Villani, M. G., Houweling, S., Dentener, F., Dlugokencky, E. J., Miller, J. B., Gatti, L. V., Engel, A., and Levin, I.: Inverse modeling of global and regional CH_4 emissions using SCIAMACHY satellite retrievals, J. Geophys. Res.-Atmos., 114, D22301, doi:10.1029/2009JD012287, 2009.

Billings, W. D., Peterson, K. M., Shaver, G. R., Trent, A. W.: Root growth, respiration, and carbon dioxide evolution in an Arctic tundra soil. Arctic Alpine Res., 9, 129–137, 1977.

Bohn, T. J., Melton, J. R., Ito, A., Kleinen, T., Spahni, R., Stocker, B. D., Zhang, B., Zhu, X., Schroeder, R., Glagolev, M. V., Maksyutov, S., Chen, G., Denisov, S. N., Eliseev, A. V., Gallego-Sala, A., McDonald, K. C., Rawlins, M. A., Subin, Z. M., Tian, H., Zhuang, Q., Kaplan, J. O.: WETCHIMP-WSL:intercomparison of wetland methane emissions models over West Siveria, Biogeosciences, 12, 3321-3349, 2015.

Brouchkov, A., Fukuda, M., Tomita, F., Asano, K., Tanaka, M.: Microbiology and gas emission at low temperatures: some field and experimental results. Tõhoku Geophys. Journ., 36, 452-455, 2003.

Bruhwiler, L., Dlugokencky, E., Masarie, K., Ishizawa, M., Andrews, A., Miller, J., Sweeney, C., Tans, P., Worthy, D.: CarbonTracker-CH_4: an assimilation system for estimating emissions of atmospheric methane, Atmos. Chem. Phys., 14, 8269-8293, 2014.

Bubier, J. L., Crill, P. M., Varner, R. K., and Moore, T. R.: BOREAS TGB-01/TGB-03 CH_4 chamber flux data: NSA Fen. Data set, available at: http://www.daac.ornl.gov, Oak Ridge, TN, USA, 1998.

Chan, K. M., Wood, R.: The seasonal cycle of planetary boundary layer depth determined using COSMIC radio occultation data, J. Geophys. Res.-Atmos., 118, 12,422-12,434, doi:10.1002/2013JD020147, 2013.

Chang, R. Y. W, Miller, C. E., Dinardo, S. J., Karion, A., Sweeney, C., Daube, B., Henderson, J. M., Mountain, M. E., Eluszkiewicz, J., Miller, J. B., Bruhwiler, L. M. P., Wofsy, S. C.: Methane emissions from Alaska in 2012 from CARVE airborne observations. Proc. Natl. Acad. Sci., 111, 16694-16699, 2014.

Chapin, F. S.: Morphological and physiological mechanisms of temperature compensation in phosphate absorption along a latitudinal gradient, Ecology, 55, 1180-1198, 1974.

Clein, J. S., Schimel, J. P.: Microbial activity of tundra and taiga soils at sub-zero temperatures. Soil. Biol. Biochem., 29(9), 1231-1234, 1995.

Clement, R. J., Verma, S. B., and Verry, E. S.: Relating Chamber Measurements to Eddy-Correlation Measurements of Methane Flux, J. Geophys. Res.-Atmos., 100, 21047–21056, 1995.

Comas, X., Slater, L., Reeve, A.: Seasonal geophysical monitoring of biogenic gases in a northern peatland: implications for temporal and spatial variability in free phase gas

Biogeosciences
Discussions

Open Access

EGU

650   production rates, J. Geophys. Res. Biogeosci. 113, G01012,
651   doi:10.1029/2007JG000575, 2008.
652 Ding, W. X., Cai, Z. C., and Wang, D. X.: Preliminary budget of methane emissions from
653   natural wetlands in China, Atmos. Environ., 38, 751–759,
654   doi:10.1016/J.Atmosenv.2003.10.016, 2004.
655 Dise, N. B.: Methane Emission from Minnesota Peatlands-Spatial and Seasonal
656   Variability, Global Biogeochem. Cy., 7, 123–142, 1993.
657 Dunfield P, Knowles R, Dumont R, Moore TR. Methane production and consumption in
658   temperate and subarctic peat soils: Response to temperature and pH. Soil Biol
659   Biochem 1993; 25: 321–326.
660 Euskirchen, E. S., Bret-Harte, M. S., Scott, G. J., Edgar, C., Shaver, G. R.: Seasonal
661   patterns of carbon dioxide and water fluxes in three representative tundra ecosystems
662   in northern Alaska, Ecosphere, 1-19, 2012.
663 Granberg, G., Ottosson-Lofvenius, M., Grip, H., Sundh, I., and Nilsson, M.: Effect of
664   climatic variability from 1980 to 1997 on simulated methane emission from a boreal
665   mixed mire in northern Sweden, Global Biogeochem. Cycles, 15, 977–991, 2001.
666 Harazono, Y., Mano, M., Miyata, A., Yoshimoto, M., Zulueta, R. C., Vourlitis, G.L.,
667   Kwon, H., Oechel, W.: Temporal and spatial differences of methane flux at arctic
668   tundra in Alaska, Natl Inst. Polar Res, Spec. Issue, 59:79–95, 2006.
669 Hargreaves, K. J., Fowler, D., Pitcairn, C. E. R. and Aurela, M.: Annual methane
670   emission from Finnish mires estimated from eddy covariance campaign
671   measurements, Theor. Appl. Climatol. 70, 203–213, 2001.
672 Henderson, J. M., Eluszkiewicz, J., Mountain, M. E., Nehrkorn, T., Chang, R. Y.-W.,
673   Karion, A., Miller, J. B., Sweeney, C., Steiner, N., Wofsy, S. C., Miller, C. E.,
674   Atmospheric transport simulations in support of the Carve in Arctic Reservoirs
675   Vulnerability Experiment (CARVE), Atmos. Chem. Phys., 15,4093-4116, 2015.
676 Hinzman, L.D., L. A. Viereck, P. Adams, V. E. Romanovsky, and K. Yoshikawa, 2006.
677   Climate and permafrost dynamics of the Alaskan boreal forest. In Alaska's changing
678   boreal forest. Edited by F.S. Chapin III, M.W. Oswood, K Van Cleve, L.A. Viereck,
679   and D.L. Verbyla. Oxford University Press, New York. pp. 39-61.
680 Hommeltenberg, J., Mauder, M., Drösler, M., Heidbach, K., Werle, P., Schmid, H. P.:
681   Ecosystem scale methane fluxes in a natural temperature bog-pine forest in southern
682   Germiny, Biogeosciences, 11, 3477-3493, 2014.
683 Hugelius, G., Strauss, J., Zubrzycki, S., Harden, J. W., Schuur, E. A. G., Ping, C.-L.,
684   Schirrmeister, L., Grosse, G., Michaelson, G. J., Koven, C. D., O'Donnell, J. A.,
685   Elberling, B., Mishra, U., Camill, P., Yu, Z., Palmtag, J., Kuhry, P.: Estimated stocks
686   of circumpolar permafrost carbon with quantified uncertainty ranges and identified
687   data gaps, Biogeosciences, 11, 6573-6593, 2014.
688 IPCC: Climate Change 2007: The Physical Science Basis. Contribution of Working
689   Group I to the Fourth Assessment Report of the IPCC, edited by: Solomon, S., Qin, D.,
690   Manning, M., Chen, Z., Marquis, M., Averyt, K. B., Tignor, M., and Miller, H. L.,
691   Cambridge University Press, Cambridge, United Kingdom and New York, 2007.
692 Iversen, C. M., Sloan, V. L., Sullivan, P. F., Euskirchen, E. S., McGuire, A. D., Norby, R.
693   J., Walker, A. P., Warren, J. M., Wullschleger, S. D.:The unseen iceberg: plant roots
694   in arctic tundra, New Phytologist, 205, 34-59, doi: 10.1111/nph.13003, 2015.
695 Iwata, H., Harazono, Y., Ueyama, M., Sakabe, A., Nagano, H., Kosugi, Y., Takahashi, K.,

Biogeosciences
Open Access
Discussions
EGU

696   Kim, Y.: Methane exchange in a poorly-drained black spruce forest over permafrost
697   observed using the eddy covariance technique, Agric. For. Meteorol., 214-215, 157-
698   168 2015.
699   Jackowicz-Korczyński, M., Christensen, T. R., Bäckstrand, K., Crill, P., Friborg, T.,
700   Mastepanov, M., Ström, L.: Annual cycle of methane emission from a subarctic
701   peatland, J. Geophys. Res., 115, G02009, doi:10.1029/2008JG000913, 2010.
702   Juutinen, S., Alm, J., Larmola, T., Huttunen, J. T., Morero, M., Martikainen, P. J.,
703   Silvola, J.: Major implication of the littoral zone for methane release from boreal
704   lakes, Global Biogeochem. Cycles, 17, 1117.10.1029/2003GB002105, 2003.
705   Karl, D. M., Tilbrook, B. D.: Production and transport of methane in oceanic particulate
706   organic matter, Nature, 368, 732-734, 1994.
707   Keller, M. M.: Biological sources and sinks of methane in tropical habitats and tropical
708   atmospheric chemistry, Princeton University, 1990.
709   King, J. Y., William, S. R., Shannon K. R.: Methane emission and transport by arctic
710   sedges in Alaska: results of a vegetation removal experiment, J. Geophys. Res., 103,
711   29083-29092.
712   Kirschke, S., Bousquet, P., Ciais, P., Saunois, M., Canadell, J. G., Dlugokencky, E. J.,
713   Bergamaschi, P., Bergmann, D., Blake, D. R., Bruhwiler, L., Cameron Smith, P.,
714   Castaldi, S., Chevallier, F., Feng, L., Fraser, A., Heimann, M., Hodson, E. L.,
715   Houweling, S., Josse, B., Fraser, P. J., Krummel, P. B., Lamarque, J., Langenfelds, R.
716   L., Le Quéré, C., Naik, V., O'Doherty, S., Palmer, P. I., Pison, I., Plummer, D.,
717   Poulter, B., Prinn, R. G., Rigby, M., Ringeval, B., Santini, M., Schmidt, M., Shindell,
718   D. T., Simpson, I. J., Spahni, R., Steele, L. P., Strode, S. A., Sudo, K., Szopa, S., van
719   der Werf, G. R., Voulgarakis, A., van Weele, M., Weiss, R. F., Williams, J. E., and
720   Zeng, G.: Three decades of global methane sources and sinks, Nat. Geosci., 6, 813–
721   823, doi: 10.1038/ngeo1955, 2013.
722   Koh, H. S., Ochs, C. A., and Yu, K. W.: Hydrologic gradient and vegetation controls on
723   CH_4 and CO_2 fluxes in a spring-fed forested wetland, Hydrobiologia, 630, 271–286,
724   doi:10.1007/S10750-009-9821-X, 2009.
725   Koven, C. D., Riley, W. J., Subin, Z. M., Tang, J. Y., Torn, M. S., Collins, W. D., Bonan,
726   G. B., Lawrence, D. M., Swenson, S. C.: The effects of vertically resolved soil
727   biogeochemistry and alternate soil C and N models on C dynamics of CLM4,
728   Biogeosciences, 10, 7109-7131, 2013.
729   Kummerow, J., Russell, M.: Seasonal root growth in the Arctic tussock tundra, Oecologia,
730   47: 196–199, 1980.
731   Lupascu, M., Wadham, J. L., Hornibrook, E. R. C., Pancost, R. D.: Temperature
732   sensitivity of methane production in the permafrost active layer at Stordalen, Sweden:
733   A comparison with non-permafrost northern wetlands, Arct., Antarc., Alp. Res., 44(4),
734   469-482, 2012.
735   Mastepanov, M., Sigsgaard, C., Tagesson, T., Ström, L., Tamstorf, M. P., Lund, M.,
736   Christensen, T. R.: Revisiting factors controlling methane emissions from high-arctic
737   tundra, Biogeosciences, 10, 5139-5158, 2013.
738   Mastepanov, M., Sigsgaard, C., Dlugokencky, E. J., Houweling, S., Ström L., Tamstorf,
739   M. P., and Christensen, T. R.: Large tundra methane burst during onset of freezing,
740   Nature, 456, 628–631, 2008.

741 Mao, J., Shi, X., Thornton, P. E., Hoffman, F. M., Zhu, Z., Myneni, R. B., Global
742   latitudinal-asymmetric vegetation growth trends and their driving mechanisms:2982-
743   2009, Remote Sens., 5 1484-1497, 2013.
744 McEwing, K. R., Fisher, J. P., Zona, D.: Environmental and vegetation controls on the
745   spatial variability of CH_4 emission from wet-sedge and tussock tundra ecosystem in
746   the Arctic, Plant Soil, 388, 37-52, 2015.
747 Melton, J. R., Wania, R., Hodson, E. L., Poulter, B., Ringeval, B., Spahni, R., Bohn, T.,
748   Avis, C. A., Beerling, D. J., Eliseev, A.V., Denisov, S. N., Hopcroft, P. O.,
749   Lettenmaier, D. P., Riley, W. J., Singarayer, J. S., Subin, Z. M., Tian, H., Zürcher,
750   Brovkin, V., van Bodegom, P. M., Kleinen, T., Yu, Z. C., Kaplan, J. O., Present state
751   of global wetland extent and wetland methane modeling: conclusions from a model
752   inter-comparison project (WETCHIMP), Biogeosciences, 10, 753–788,2013.
753 Meng, L., Hess, P. G. M., Mahowald, N. M., Yavitt, J. B., Riley, W. J., Subin, Z. M.,
754   Lawrence, D. M., Swenson, S. C., Jauhiainen, J., and Fuka, D. R.: Sensitivity of
755   wetland methane emissions to model assumptions: application and model testing
756   against site observations, Biogeosciences, 9, 2793–2819, doi:10.5194/bg-9-2793-
757   2012, 2012.
758 Mialon, A., Royer, A., Fily, M.: Wetland seasonal dynamics and interannual variability
759   over northern high latitudes, derived from microwave satellite data, J. Geophys. Res.,
760   110, D17102, doi:10.1029/2004JD005697, 2005.
761 Moosavi, S. C., Crill, P. M., Pullman, E. R., Funk, D. W., Peterson, K. M.: Controls on
762   CH_4 flux from an Alaskan boreal wetland, Global Biogeochem. Cycles, 10, 287-296,
763   1996.
764 Morin, T. H., Bohrer, G., Naor-Azrieli, L., Mesi, S., Kenny, W. T., Mitsch, W. J.,
765   Schäfer, K. V. R.: The seasonal and diurnal dynamics of methane flux at a created
766   urban wetland. Ecol. Engin., 72, 74-83, 2014.
767 Nakano, T., Kuniyoshi, S., Fukuda, M.: Temporal variation in methane emission from
768   tundra wetlands in a permafrost area, northeastern Siberia. Atmos. Environ., 34, 1205–
769   1213, 2000.
770 Olivas, P. C., Oberbauer, S. F., Tweedie, C., Oechel, W. C., Lin, D., Kuchy, A.: Effects
771   of Fine-Scale Topography on CO_2 Flux Components of Alaskan Coastal Plain Tundra:
772   Response to Contracting Growing Seasons, Arct. Antarct. Alpine Res., 43, 256–266,
773   doi: 10.1657/1938-4246-43.2.256, 2011.
774 Peters, W., Jacobson, A. R., Sweeney, C., Andrews, A. E., Conway, T. J., Masarie, K.,
775   Miller, J. B., Bruhwiler, L. M. P., Petron, G., Hirsch, A., Worthy, D. E. J., van der
776   Werf G. R., Randerson, J. T., Wennberg, P. O., Krol, M. C., Tans, P. P.: An
777   Atmospheric perspective on north American carbon dioxide exchange:
778   CarbonTracker, PNAS, 18925-18930, 2007.
779 Pickett-Heaps, C. A., Jacob, D. J., Wecht, K. J., Kort, E. A., Wofsy, S. C., Diskin, G. S.,
780   Worthy, D. E. J., Kaplan, J. O., Drevet, J.: Magnitude and seasonality of wetland
781   methane emissions from the Hudson Bay Lowlands (Canada), Atmos. Chem. Phys.,
782   11, 3773-3779, 2011.
783 Prigent, C., F. Papa, F. Aires, W. B. Rossow, E. Matthews.: Global inundation dynamics
784   inferred from multiple satellite observations, 1993-2000, J. Geophys. Res.-Atmos.,
785   112, D12107, doi:10.1029/2006JD007847, 2007.
786 Qian, T. T., Dai, A., Trenberth, K. E., and Oleson, K. W.: Simulation of global land

787   surface conditions from 1948 to 2004. Part I: Forcing data and evaluations, J.
788   Hydrometeorol., 7, 953–975, 2006.
789   Riley, W. J., Subin, Z. M., Lawrence, D. M., Swenson, S. C., Torn, M. S., Meng, L.,
790   Mahowald, N. M., Hess, P.: Barriers to predicting changes in global terrestrial
791   methane fluxes: analyses using CLM4Me, a methane biogeochemistry model
792   integrated in CESM, Biogeosciences, 8, 1025-1953, 2011.
793   Ringeval, B., de Noblet-Ducoudré, N., Ciais, P., Bousquet, P., Prigent, C., Papa, F.,
794   Rossow, W. B.: An attempt to quantify the impact of changes in wetland extent on
795   methane emissions on the seasonal and interannual time scales, Global Biogeochem.
796   Cycles, 24, GB2003, doi:10.1029/2008GB003354, 2010.
797   Rinne, J., Riutta, T., Pihlatie, M., Aurela, M., Haapanala, S., Tuovinen, J., Tuittila, E.:
798   Annual cycle of methane emission from a boreal fen measured by the eddy Covance
799   technique., Tellus, 59B, 449-457, 2007.
800   Roulet, N. T., Ash, R., Moore, T.R.: Low boreal wetlands as a source of atmospheric
801   methane, J. Geophys. Res., 97 (D4), 3739-3749, 1992.
802   Saarnio, S., Alm, J., Silvola, J., Lohila, A., Nykanen, H., and Martikainen, P. J.: Seasonal
803   variation in CH_4 emissions and production and oxidation potentials at microsites on an
804   oligotrophic pine fen, Oecologia, 110, 414–422, 1997.
805   Schroeder, R., McDonald K. C., Champan, B.D., Jensen, K., Podest, E., Tessler, Z. D.,
806   Bohn, T. J., Zimmermann, R.: Development and evaluation of a multi-year fractional
807   surface water data set derived from active/passive microwave remote sensing data, 7,
808   16688-16732, 2015.
809   Schütz, H., Seiler, W., Conrad, R.: Influence of soil-temperature on methane emission
810   from rice paddy fields, Biogeochemistry, 11, 77–95, 1990.
811   Segers, R.: Methane production and methane consumption: a review of process
812   underlying wetland methane fluxes, Biogeochemistry, 41, 23-51,1998.
813   Shannon, R. D. and White, J. R.: 3-Year Study of Controls on Methane Emissions from 2
814   Michigan Peatlands, Biogeochemistry, 27, 35–60, 1994.
815   Siavoshi., M., Dastan, S., Yassari, E., Laware, S. L.: Role of organic fertilizers on
816   morphological and yield parameters in rice (Oryza sativa L.), Intl. J. Agron. Plant
817   Prod., 4, 1220-1225, 2013.
818   Sloan, V.: Plant roots in Arctic ecosystems: stocks and dynamics and their coupling to
819   aboverground parameters, *PhD Thesis. University of Sheffield,* Sheffield, UK, 2011.
820   Smith, L. K., Lewis, W. M., Chanton, J. P., Cronin, G., and Hamilton, S. K.: Methane
821   emissions from the Orinoco River floodplain, Venezuela, Biogeochemistry, 51, 113–
822   140, 2000.
823   Song, C., Xu, X., Sun, X., Tian, H., Sun, L., Miao, Y., Wang, X., Guo, Y.: Large
824   methane emission upon spring thaw from natural wetlands in the northern permafrost
825   region, Environ. Res. Lett., 7, 034009, doi:10.1088/1748-9326/7/3/034009, 2012.
826   Starr, G., Oberbauer, S., Ahlquist, L.: The photosynthetic response of Alaskan tundra
827   plants to increased season length and soil warming, Arct. Antarct. Alp. Res. 40(1),
828   181–191, 2008.
829   Sturtevant, C. S., Oechel, W. C., Zona, D., Kim, Y., and Emerson, C. E.: Soil moisture
830   control over autumn season methane flux, arctic coastal plain of Alaska,
831   Biogeosciences, 9, 1423–1440, 2012.

Biogeosciences
Open Access
Discussions
EGU

832 Sullivan, P. F., Welker, J. M.: Warming chambers stimulate early season growth of an
833   arctic sedge: results of a minirhizotron field study, Oecologia, 142, 616-626, 2005.
834 Svensson, B. H., Christensen, T. R., Johansson, E., and Oquist, M.:Interdecadal changes
835   in CO_2 and CH_4 fluxes of a subarctic mire:Stordalen revisited after 20 years, Oikos, 85,
836   22–30, 1999.
837 Tian, Y, Dickinson, R. E., Zhou, L., Zeng, X., Dai, Y., Myneni, R. B., Knyazikhin, Y.,
838   Zhang, X., Friedl, M., Yu, H., Wu, W., Shaikh, M.: Comparison of seasonal and
839   spatial variations of leaf area index and fraction of absorbed photosynthetically active
840   radiation from Moderate Resolution Imaging Spectroradiometer (MODIS) and
841   Common Land Model, J. Geophys. Res.,109, D01103, doi:10.1029/2003JD003777,
842   2004.
843 Tokida, T., Mizoguchi, M., Miyazaki, T., Kagemoto, A., Nagata, O., Hatano, R.:
844   Episodic release of methane bubbles from peatland during spring thaw, Chemosphere,
845   70, 165-171, 2007.
846 Torn, M. S., and Chapin III, F. S.: Environmental and biotic controls over methane flux
847   from arctic tundra, Atmos. Environ., 32, 3201–3218, 1993.
848 van Fischer, J. C., Rhew, R. C., Ames, G. M., Fosdick, B. K., von Fischer, P. E.:
849   Vegetation height and other controls of spatial variability in methane emissions from
850   the Arctic coastal tundra at Barrow, Alaska, J. Geophys. Res., 115, G00I03,
851   doi:10.1029/2009JG001283, 2010
852 van Hulzen J.B., Segers, R., van Bodegom, P. M., Leffelaar, P.A.: Temperature effects on
853   soil methane production: and explanation for observed variability, Soil Biol. and
854   Biochem., 31, 1919-1929, 1999.
855 van Winden, J. F., Reichart, G.-J., McNamara, N. P., Benthien, A., Damsté, J. S. S.:
856   Temperature-induced increase in methane release from peat bogs: a mesocosm
857   experiment, PLoS ONE 7(6): e39614. doi:10.1371/journal.pone.0039614, 2012.
858 Verma, A., Arkebauer, T. J., and Valentine, D.: BOREAS TF-11 CO_2 and CH_4 flux data
859   from the SSA-Fen. Data set, available at: http://www.daac.ornl.gov, Oak Ridge, TN,
860   USA, 1998.
861 Walter, K. M., Zimov, S. A., Chanton, J. P., Verbyla, D., Chapin III, F. S.: Methane
862   bubbling from Siberian thaw lakes as a positive feedback to climate warming, Nature,
863   443, 71-75, dio: 10.1038/nature0504, 2006.
864 Wang, C., Xiao, S., Li, Y., Zhong, H., Li, X., Peng, P.: Methane formation and
865   consumption processes in Xiangxi Bay of the Three Gorges Reservoir, Sci. Rep. 4,
866   444, doi:10.1038/srep04449, 2014.
867 Wania, R., Ross, I., and Prentice, I. C.: Implementation and evaluation of a new methane
868   model within a dynamic global vegetation model: LPJ-WHyMe v1.3.1, Geosci. Model
869   Dev., 3, 565–584, doi:10.5194/gmd-3-565-2010, 2010.
870 Wassmann, R., Thein, U. G., Whiticar, M. J., Rennenberg, H., Seiler,W., and Junk,W. J.:
871   Methane emissions from the Amazon floodplain: Characterization of production and
872   transport, Global Biogeochem. Cy., 6, 3–13, 1992.
873 Whalen, S. C., Reeburgh, W. S.: Consumption of atmospheric methane by tundra soils,
874   Nature, 342, 160–162, 1990.
875 Whalen, S. C. and Reeburgh,W. S.: Interannual variations in tundra methane emission: a
876   4-year time series at fixed sites., Global Biogeochem. Cy., 6, 139–159, 1992.

Biogeosciences
Discussions

Open Access

EGU

877   Whiting, G. J., Chanton, J. P.: Greenhouse carbon balance of wetlands: Methane
878   emission versus carbon sequestration, Tellus, 53B, 521-528, 2001.
879   Wickland, K. P., Striegl, R. G., Schmidt, S. K., Mast, M. A.: Methane flux in subalpine
880   wetland and unsaturated soils in the southern Rocky Mountains, Global Biogeochem.
881   Cycles, 13, 101–113, 1999.
882   Wilson, J. O., Crill, P. M., Bartlett, K. B., Sebacher, D. I., Harriss, R. C., Sass, R. L.:
883   Seasonal variation of methane emissions from a temperate swamp, Biogeochemistry,
884   8, 55-71, 1998.
885   Yvon-Durocher, G., Montoya, J. M., Woodward, G., Jones, J. I., Trimmer, M.: Warming
886   increases the proportion of primary production emitted as methane from freshwater
887   mesocosms, Global Chang. Biol., 17, 1225-1234, 2011.
888   Yvon-Durocher, G., Allen, A. P., Bastviken, D., Conrad, R., Gudasz, C., St-Pierre, A.,
889   Thanh-Duc, N., del Giorgio, P. A.: Methane fluxes show consistent temperature
890   dependence across microbial to ecosystem scale, Nature, 507, 488-491, 2014.
891   Zhuang, Q., Melillo, J. M., Kicklighter, D. W., Prinn, R. G., McGuire, A. D., Steudler, P.
892   A., Felzer, B. S., and Hu, S.: Methane fluxes between terrestrial ecosystems and the
893   atmosphere at northern high latitudes during the past century: A retrospective analysis
894   with a process based biogeochemistry model, Glob. Biogeochem. Cycles, 18,
895   GB3010, doi:3010.1029/2004GB002239, 2004.
896   Zona, D., Oechel, W. C., Kochendorfer, J., Paw U, Salyuk, A. N., Olivas, P. C.,
897   Oberbauer, S. F., Lipson, D. A.: Methane fluxes during the initiation of a large-scale
898   water table manipulation experiment in the Alaskan Arctic tundra, Global
899   Biogeochem. Cycle 23, GB2013, doi:10.1029/2009GB003487, 2009.
900   Zona, D., Gioli, B., Commane, R., Lindaas, J., Wofsy, S. C., Miller, C. E., Dinardo, S. J.,
901   Dengel, S., Sweeney, C., Karion, A., Chang, R.Y.-W., Henderson, J. M., Murphy, P.
902   C., Goodrich, J. P., Moreaux, V., Liljedahl, A., Watts, J. D., Kimball, J. S., Lipson, D.
903   A., Oechel, W. C.: Cold season emissions dominate the Arctic tundra methane budget,
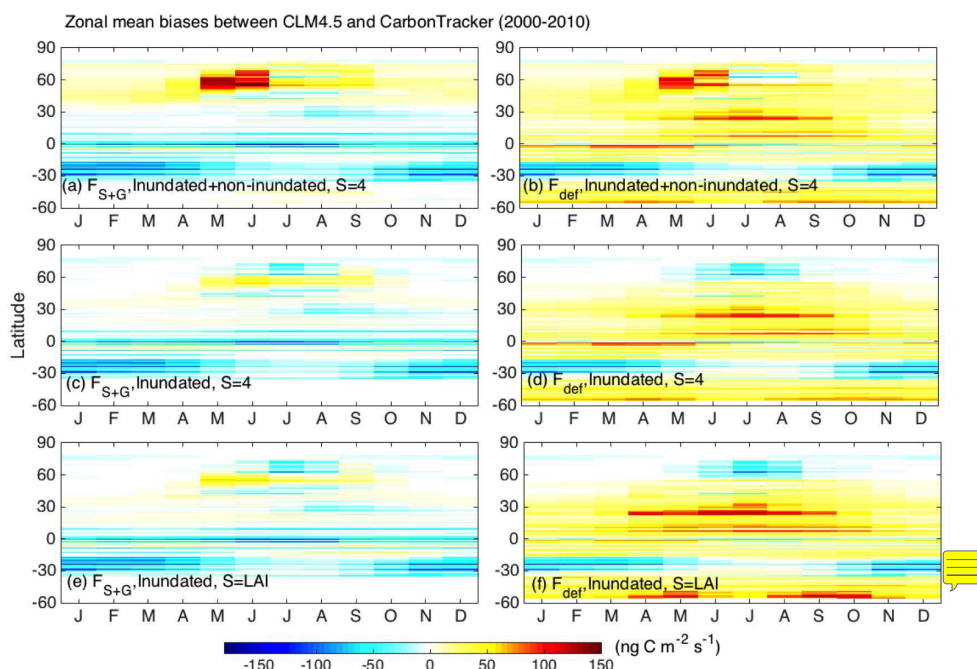904   PNAS, 113,40-45, 2016.

Fig. 1. Zonal mean biases of CH$_4$ emissions between CLM4.5 predictions and CarbonTracker (CH$_4$_CLM4.5-CH$_4$_CarbonTracker) with SWAMPS-GLWD (F_{S+G}) and CLM4.5 predicted (F_{def}) inundation fraction: CLM4.5 predictions of both inundated and noninundated emissions with F_{S+G} (a) and F_{def} (b), while aerechyma area is corrected with S=4; CLM4.5 predictions of inundated emissions only with F_{S+G} (c) and F_{def} (d), while aerechyma area is corrected with S=4; CLM4.5 predictions of inundated emissions only with F_{S+G} (e) and F_{def} (f), while aerechyma area is parameterized by default S=LAI.
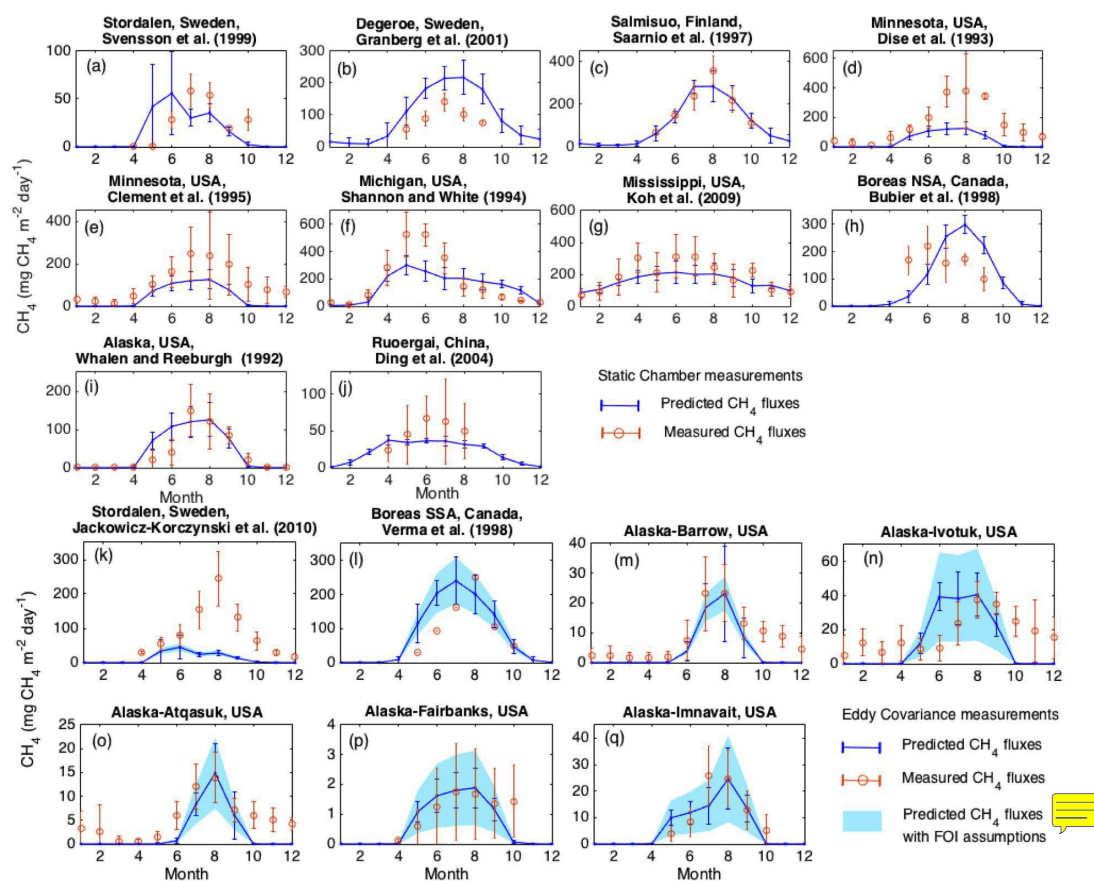
Fig. 2. Comparison of monthly mean simulated net CH_4 flux between 2000 and 2012 and observed monthly mean net CH_4 emissions in measurement year(s). The site measurements with static chamber are shown in (a-j) and measurements with eddy covariance (EC) towers are shown in (k-q). The error bars are standard deviation of monthly mean. The measurements with EC tower are weighted with a range of inundation fraction based on best estimates available: Stordalen: 80-100%; Boreas SSA: 50-90%; Alaska-Barrow: 60-100%, Alaska-Atqasuk: 10-30%; Alaska-Ivotuk: 5-25%; Alaska-Fairbanks:0.5-2.5%, Alaska-IMN:5-25%. Detailed description of the sites and measurements are shown in Table S1.
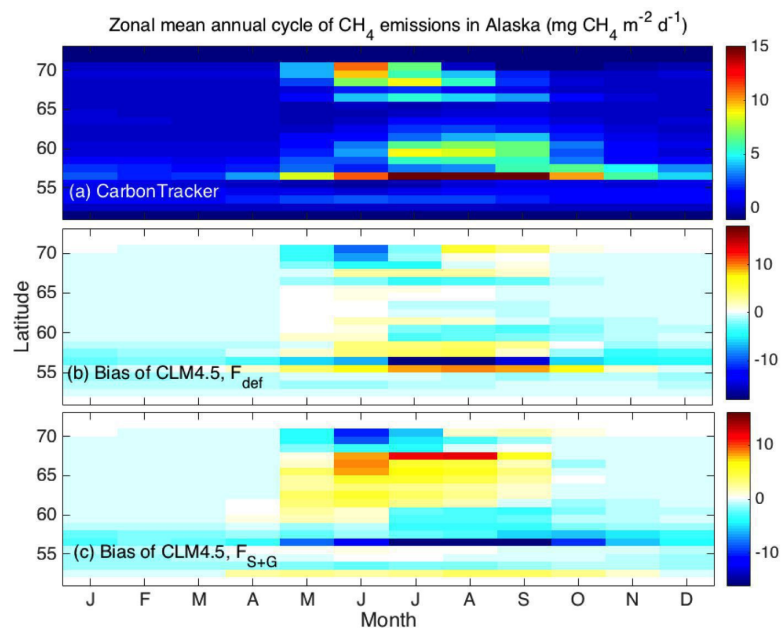
Fig. 3. The 2000-2010 zonal mean annual cycle of CH_4 emission (mg CH_4 m^{-2} day^{-1}) across Alaska predicted by CarbonTracker (a), and biases of CLM4.5 with CLM4.5 predicted inundation fraction (F_{def}) (b) and SWAMPS-GLWD inundation fraction (F_{S+G}) (c) . The 0.5°×0.5° CLM4.5 is regridded to 1°×1° to be consistent with CarbonTracker.
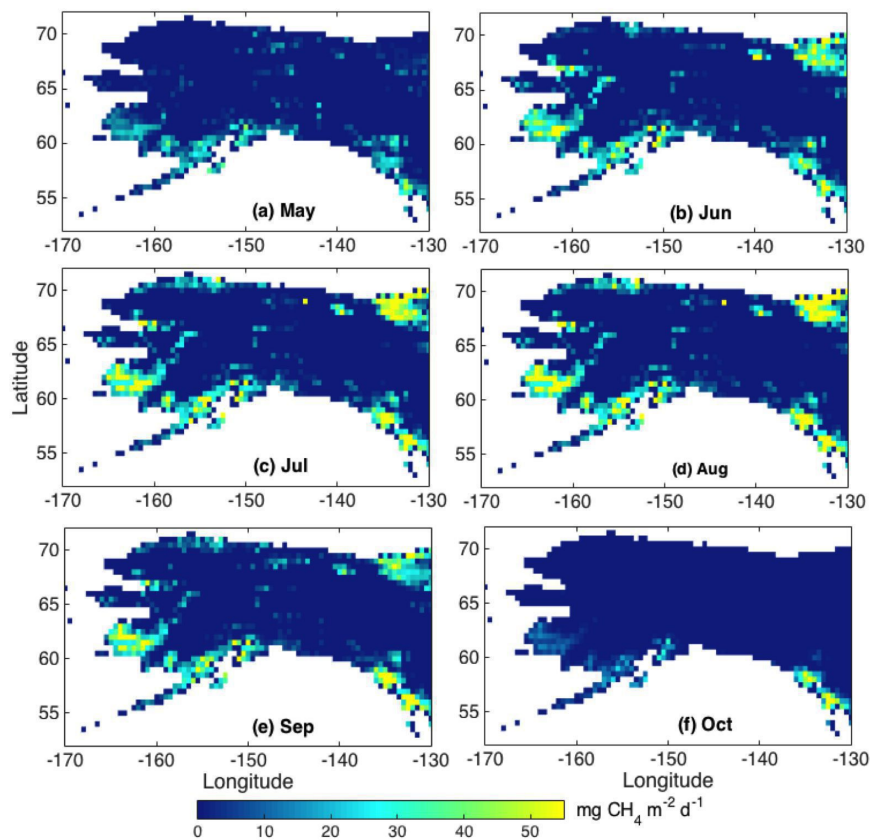
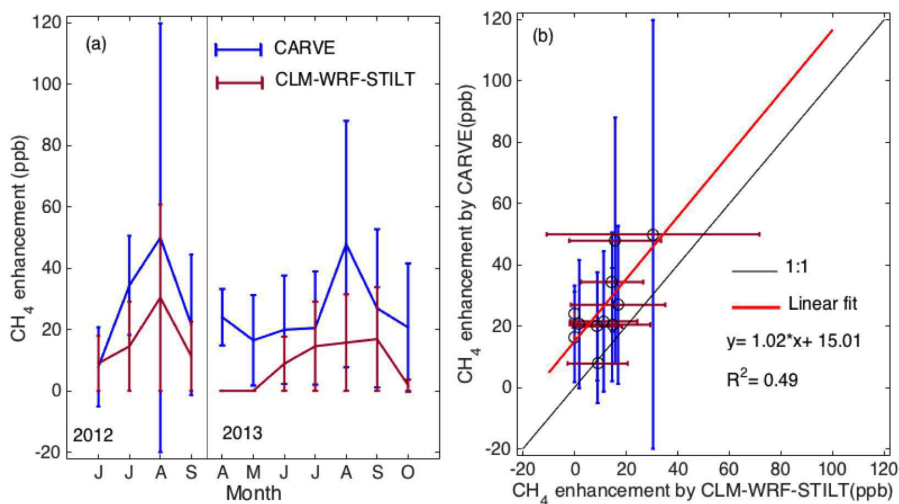Fig. 4. CLM4.5 simulated mean monthly CH_4 emissions with F_{def} across years 2000-2012.

Fig. 5. The monthly mean atmospheric mole fraction enhancements in CH_4 estimated by WRF-STILT-CLM4.5 and CARVE measurements. (a) Observed and simulated monthly CH_4 mole fraction enhancements in 2012 and 2013; (b) Linear regression of measured versus modeled CH_4 mole fraction enhancements. The error bars are standard deviation of monthly mean.
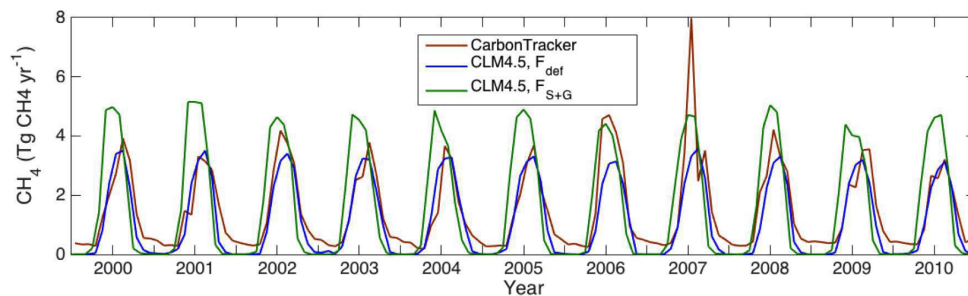
Fig. 6. Time variation of integrated CH_4 ($Tg\ CH_4\ yr^{-1}$) emissions from Alaska by CarbonTracker (brown), CLM4.5 with internally-predicted fraction of inundation F_{def} (blue) and CLM4.5 SWAMPS-GLWD fraction of inundation F_{S+G} (green).
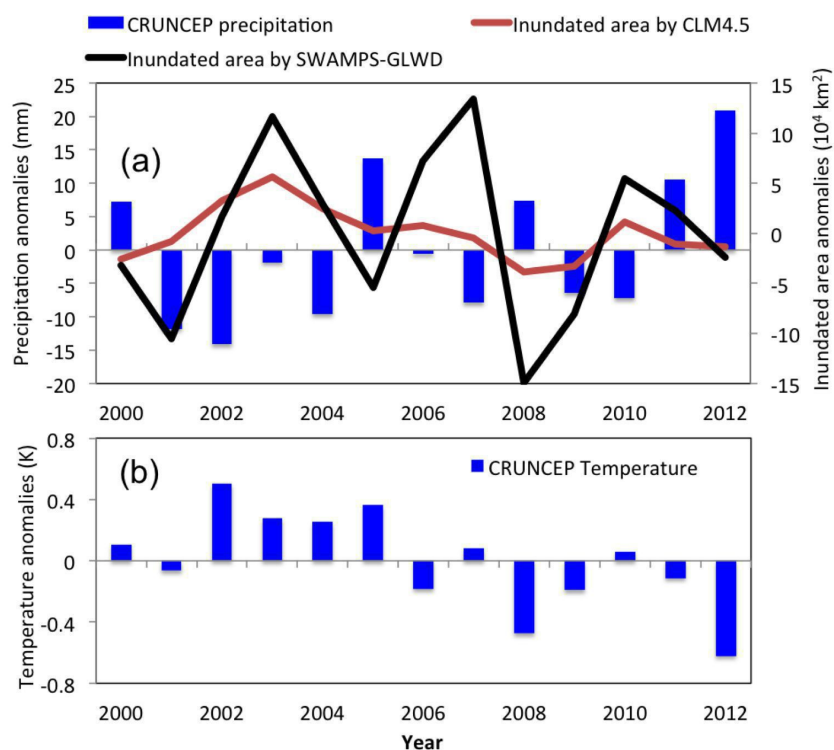
Fig. 7. The anomalies of annual precipitation and inundated area in Alaska (a) and the anomalies of annual mean temperature (b). The anomalies are calculated by subtracting the average between 2000-2012.
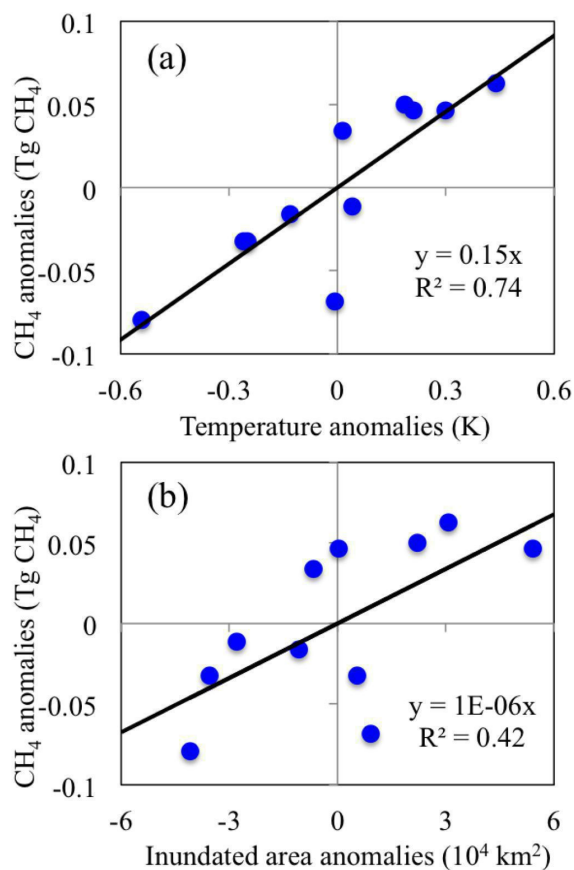
Fig. 8. The correlation between CLM-predicted annual CH_4 emission anomalies and mean annual temperature anomalies (a) and correlation between annual CH_4 emission anomalies and predicted inundated area anomalies during 2000-2010. The anomalies are calculated by subtracting the average between 2000-2010.